Spatiotemporal Operational Emissions Associated with Light-, Medium-, and Heavy-Duty Transportation Electrification

Jessica L. Wert*, *Student Member, IEEE,* Farnaz Safdarian*, *Member, IEEE,*
Diana Wallison, *Student Member, IEEE,* Jung Kyo Jung, *Student Member, IEEE,*
Yijing Liu, *Member, IEEE,* Thomas J. Overbye, *Fellow, IEEE,* Yanzhi Xu

***Abstract*—The spatiotemporal distribution of pollutants plays a significant role on their impact on ecosystems and human health. This paper presents a strategy for calculating spatiotemporal operational emissions of road transportation and the electric grid to quantify the impact of transportation electrification. Emissions from internal combustion engine vehicles and offset emissions from electric vehicles (EVs) are considered using actual transportation networks and travel data. The spatiotemporal charging demand for light-duty and medium- and heavy-duty EVs are estimated in a behaviorally-informed way and mapped to electrical buses within the power grid and an ac optimal power flow with unit commitment is solved. The methodology is demonstrated with ten scenarios simulated on a grid with 7000 electrical buses geographically sited in Texas, created with actual generator data for the 2020 grid, and a future case including anticipated generator updates by 2030. Results show overall transportation emissions reductions in daily operational emissions of up to 20–30% for all pollutants studied, outweighing the increase in emissions from the electric grid. Considering emissions on an hourly basis, up to approximately 1000% reduction in CO emissions is observed.**

***Index Terms*—Electric Vehicles, Emissions, Power Systems, Transportation, Charging**

I. Introduction

NEARLY one-third of global emissions are attributed to the transportation sector [1]. In contrast to conventional cars with internal combustion engines (ICEs) that produce harmful emissions, electric vehicles (EVs) produce no direct tailpipe emissions and have been extensively recognized as a key solution to environmental concerns, to control oil usage, and to achieve net-zero emissions in the road transportation sector. Indirectly, however, EVs add electricity demand to the grid during charging, resulting in increased generation required in the electric grid and, in turn, the potential of additional emissions.

The main pollutants of concern from transportation and power plants include carbon dioxide (CO_2), nitrous oxides (NO_x), particulate matter ($PM_{2.5}$), volatile organic compounds (VOCs), and carbon monoxide (CO) [2]. Each of these pollutants has consequences on either the environment or public health. The spatiotemporal distribution of $PM_{2.5}$ determines its intensity, thus the specific locality and timing of emission is an important consideration when evaluating its impact. CO_2 and CO have a more global impact and are contributors to climate change [3]. CO is also able to modulate the production of methane and tropospheric ozone (O_3) [4]. O_3 is a type of photochemical oxidant, which is formed in the troposphere with complex non-linear processes among interaction of NO_x, VOC, temperature, and intensity of solar radiation [5], [6], and creates issues for ecosystems [7] and human respiratory health [8]. Therefore, understanding the spatiotemporal distribution of VOC, NO_x, CO, and $PM_{2.5}$ is important when determining the production of methane and O_3. Power plants that are far away from large cities and polluted areas have a less negative impact. Therefore, it is crucial to study the changes in power plant generation dispatch from incorporating EV charging demand to ascertain the spatiotemporal impact of EVs on operational emissions.

A. Policies and Limitations on Emissions

The shift towards the increased prevalence of EVs is motivated by environmental policies. The main environmental policies rely on three strategies: carbon pricing, technology subsidies, and performance standards. Carbon pricing policies provide a direct financial incentive to reduce emissions, and they are implemented through tax or fees, or through the establishment of a market-based cap-and-trade system. Technology subsidies provide incentives for low-emission technology deployment and are implemented through tax credits or direct public funding. Performance standards require specific products or processes to meet certain minimum or average levels of technical performance and range from being flexible, broad, and market-based, to be prescriptive and site-specific. Procurement policies, international agreements, and a wide array of other programs also play important roles in a comprehensive climate policy portfolio [9].

The level of hazard of the pollutants studied could be characterized using permissible exposure limit (PEL) and permissible exposure time (PET). The more hazardous the pollutant, the smaller the PEL and PET. Table I presents the PELs and PETs of the studied pollutants. The PEL and

*The first two authors of this paper contributed equally to this project.

J. Wert, F. Safdarian, D. Wallison, J.K. Jung, Y. Liu, and T. Overbye are with the Department of Electrical and Computer Engineering at Texas A&M University, College Station, TX, USA. Y. Xu is with ElectroTempo, Arlington, VA, USA (e-mail: jwert@tamu.edu, fsafdarian@tamu.edu).

TABLE I:
Permissible Exposure Limit (PEL) and Permissible Exposure Time (PET)

	VOC	NO_x	$PM_{2.5}$	CO_2	CO
PEL (ppm)	0.5–0.75 [10]	25 [11]	0.035 [12]	5,000 [13]	50 [14]
PET (hour)	8–10 [15]	8 [11]	24 [12]	8 [13]	8 [14]

PET of VOC is variable depending on the activity level of the individuals exposed, with more active individuals being at greater risk of adverse effects.

B. Literature Review

Several studies in the literature focus on the impact of EVs on the environment. Study [16] reviews the environmental benefits of transportation electrification with a focus on urban buses and offers empirical guidance to policymakers considering investments in this section. Reference [17] analyzes the role of transportation electrification in the context of energy system transformation and climate stabilization. Reference [18] focuses on electrification of government, commercial, and industrial fleets and studies the technology and market assessment of transportation sector. Since medium- and heavy-duty vehicles are responsible for a significant portion of greenhouse gas emissions and harmful particulate emissions, reference [19] provides an overview of the current and future state of electrifying this sector. Reference [20] studies and offers suggestions to support the actualization of benefits for environmental justice communities through the implementation of transportation electrification. This reference also provides additional clarity for policymakers in creating regulations that best serve their needs.

Several references study different parts of the supply chain for EV integration and proceed well-to-wheels analysis for using EV versus ICE. A well-to-wheels analysis [21] compares different passenger vehicles based on three key indicators: petroleum energy use, CO_2 emissions, and economic cost is studied in several countries. Authors concluded that the well-to-wheels emissions from electric vehicles greatly varies depending on the generation mix or the amount of renewable generation in the case study [21]. In [22], the authors analyzed the extent to which the lowering greenhouse gas emissions associated with EVs differs among 70 countries in the world, in relation to their domestic electricity generation mix and concluded that countries with a high percentage of fossil fuels in their electricity generation mix have higher greenhouse gas emissions for EVs, and even for some of these countries, EVs were associated with more greenhouse gas emissions than ICEs. In [23], the city of Beijing in China is studied as an important hub for possible EV promotion and air pollution issues with 2015 electricity generation mix and the predicted 2030 generation mix and the impact of light-duty EVs in well-to-wheel emissions are studied. Authors of [24] propose an EV emission approximation to calculate operational emissions of grid and EVs using hourly data.

C. Contributions

Although many papers in the literature study the impact of EVs on emissions, there is no prior reference to the study of a large, industry-size realistic grid using actual generators' data and actual transportation data for the calculation of the spatiotemporal impact of ICEs as well as light-duty (LD) and medium- and heavy-duty (MHD) EVs on large cities. In this paper, the spatiotemporal operational emissions are calculated based on a comparison of emissions from ICEs and replacing a variety of possible ranges of conventional ICE vehicles with EVs in the current electric grid and future electric grid with an increased penetration of renewable resources. The proposed strategy can be implemented to any other industrial case and can have applications in evaluating the impact of emissions reduction policies. To choose possible scenarios for future EV penetrations, several references are studied. According to [25], it is estimated that global EV sales will grow by 39% annually and will increase up to 30 million in 2028, which will represent around 50% of new car sales in 2030. Also, California recently passed legislation to ban light-duty internal combustion vehicle sales by 2035 [26]. This puts the state on a faster EV sales curve than [27]. Based on an established vehicle adoption model [28], a sales curve according to CA's legislation will result in about 20% of the light-duty vehicle population being EVs by 2029. Overall, it is also expected that 26.4 million EVs are projected on U.S. roads by 2030, which includes 10% of the 259 million light-duty vehicles [29]. Meanwhile, commercial medium- and heavy-duty (MHD) vehicles are also transitioning to EVs. Reference [30] estimates that EVs will make up about 10% of all MHD vehicles by 2030. Based on these predictions two different EV penetrations are used for simulations in this paper. One goal of this paper is to show the hourly impact of LD and MHD EVs on a realistic coupled-infrastructure model incorporating realistic transportation network and electric grid models. The emissions from the electric power grid generation are considered, accounting for hourly increase of electrical load for EV charging, in addition to the transportation emissions. Realistic charging patterns of LD and MHD EVs are created using actual transportation data of the greater Houston region in Texas, United States. The EV charging loads are then mapped to a realistic synthetic grid on the footprint of Texas. This study is performed on the synthetic grid in Texas [31] as a case study that is created based on actual generators' data from the year 2020 and the predicted generation mix in 2030 based on an assessment made by the Electric Reliability Council of Texas (ERCOT) [32], accounting for changes in the penetration of renewable resources and results are presented. Since the actual travel data is used for estimating the required charging demand for EVs and the generators, which are the main sources of emissions from EVs are based on actual generators' data, the study results are realistic and the proposed strategy can be implemented in any other case study. Nevertheless, the Texas region serves as an interesting case study because the Texas transmission grid is a large grid with nearly 7000 electrical nodes, called "buses," and is independent of all other parts of the U.S. and the impact of EV charging can be studied more

precisely. ERCOT is facing an extended increase in EVs and since the electric grid over Texas footprint is separated from the rest of U.S., this grid is a suitable case for EV studies. This is the first study to provide spatiotemporal emissions calculations for the grid and transportation networks at this spatiotemporal resolution and highlights specific pollutants including NO_x, $PM_{2.5}$ and VOC for which their distribution is a crucial consideration for their impacts on human health and the environment. The methodology is summarized in Figure 1. In summary, the main contributions of this paper are:

- Reviewing the main pollutants from transportation and electrical sectors and the significance of their spatiotemporal distribution on human health
- Creating a coupled-infrastructure model of transportation network and electrical grid based on publicly-available data such as generators and road data
- Calculating a detailed spatial and temporal impact of ICEs on harmful emissions and O_3 creation
- Calculating detailed spatial and temporal emissions from LD and MHD EV charging demand related to O_3 creation
- Showing the importance of direct inclusion of weather data (varying with location and time) in power system models when quantifying operational emissions
- Simulating the impact of added charging demand from different types of EVs (LD, MHD) with behaviorally-informed charging patterns on the grid
- Visualizing the locations and scale of impact of EVs on the electrical grid emissions
- Visualizing the temporal impact of EVs on hourly graphs

II. Modeling EVs in the Grid

A. Modeling EV Charging Demand

1) Traffic Modeling: The traffic modeling used in this paper is performed using the 2020 regional Travel Demand Model (TDM) obtained from the Houston-Galveston Area Council [33]. TDMs are typically used in the regional transportation planning process. TDMs contain trip origin-destination matrices by vehicle type (light- versus medium- and heavy-duty vehicles) for multiple time periods throughout a typical day within the regional transportation network, along with the trip distances, travel times, and speeds. The information from the TDM is used to estimate the on-road energy consumption of vehicles. The classification of light-, medium-, and heavy-duty vehicles is based on the United States Environmental Protection Agency's Motor Vehicle Emission Simulator (MOVES). Light-duty vehicles are passenger cars and light trucks. Medium- and heavy-duty trucks are single-unit, refuse, and combination trucks.

2) Light-Duty Electric Vehicle Charging Load Modeling: Possible charging scenarios of integrated modeling of LD EVs are proposed and explained in [34] and [35]. Based on existing literature [36], we assume an uncontrolled charging scenario where most EVs are charged at home and overnight using a level 1 charger, which is the most affordable from the charging infrastructure perspective. In this model it is assumed that locations of charging stations are at homes and ending travel of the day locations.

3) Medium- and Heavy-Duty EV Charging Load Modeling: Given the current technological and commercial availability of medium- and heavy-duty (MHD) vehicles and the related charging infrastructure, this paper considers short-haul MHD vehicles charging only at their depots. MHD vehicle charging demand is simulated based on vehicle miles traveled (VMT), obtained from the TDM, electric MHD vehicle fuel economy, assembled from online specification sheets of about 100 electric truck models, and the likelihood of trips ending at depots by truck type and time of day, estimated from a Bayesian Network Model based on a Commercial Vehicle Survey [37]. We assume that the vehicles are charged with 100 kW level 3 chargers, given the fact that level 2 chargers are not likely to meet the operational requirements of heavier vehicles [38].

B. Mapping EV Load to the Transmission System

Once the transportation network with charging locations is established and EV loads are calculated, the geographic information from the electric grid is leveraged to map the EV charging load to the appropriate transmission-level substations. The mapping methodology used was developed in [34]. The mapping takes the locations of the transmission substations and creates tessellating service areas using Voronoi polygons such that the nodes are central within their respective service areas.

The process of this mapping for purely transmission-level simulation is as follows:

1) Using the transmission substation geographic coordinates, create Voronoi polygons to represent the service area of each substation.
2) For each EV charging location, determine in which substation service area the charging station lies.
3) Add a load to the electric grid model for the EV charging load to be added to the system.

C. Load Time Series

The hourly time series of bus-level load for a year are created based on the strategy explained in previous work [39], [40]. For the load time series, the geographic coordinates of each bus are used to determine a unique electricity consumption profile at that location. An iterative aggregation approach is then taken to integrate publicly available building- and facility-level load time series to the bus-level. This approach leverages the composition ratio of residential, commercial, and industrial loads at each node in the system as well as location-specific prototypical building and facility-level load time series to develop the node-level load time series. The synthetic load time series were validated using time series from the actual power systems in [40].

Once the load from each EV charging station is mapped to its substation within the transmission system, the EV load time series from Section II-A is represented as a load at bus level within its assigned substation. This load is then added to the bus-level synthetic load time series.

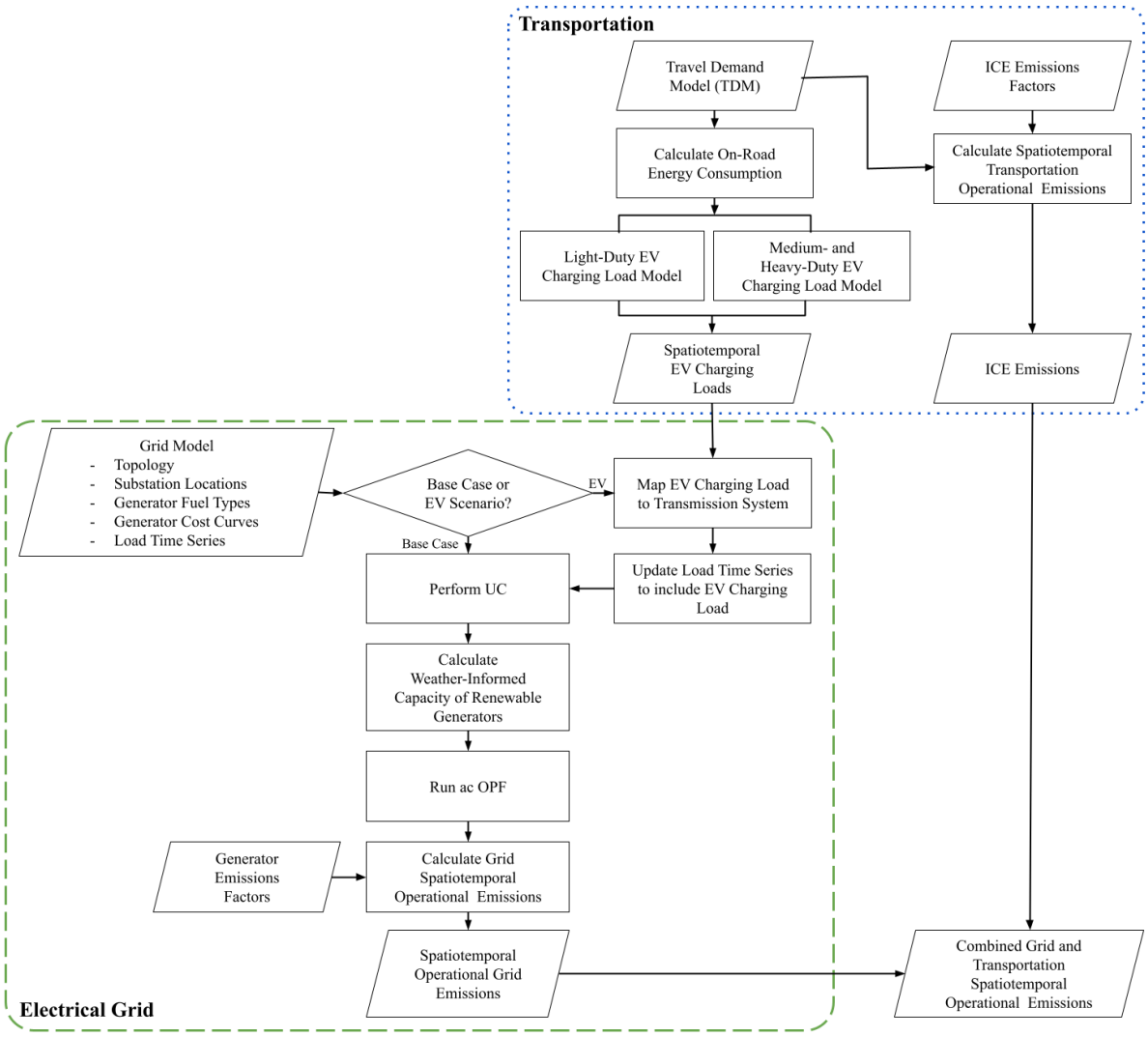

Fig. 1: Workflow of the Calculation of the Combined Spatiotemporal Operational Emissions of the Electric Grid and Transportation Networks

III. Time Step Simulation

For each scenario, unit commitment (UC) was performed to determine which generators in the electrical grid would be online using generator cost curves, and an ac optimal power flow (OPF) was solved for every hour within the 24-hour period of simulation, providing cost-optimized dispatch of generators on an hourly basis feasible within the operational constraints of the system.

A. Unit Commitment

Unit Commitment (UC) determines if each generating unit is on or off at each time interval of the study [41]–[43]. Using binary variables for the on/off status of generating units is proposed in the literature for dc OPF [44]. The dc OPF with UC is a mixed-integer linear programming (MILP) and has created challenges as it is computationally expensive for larger cases since the size of the optimization problem also grows non-linearly with the size of variables [45].

However, in this paper to have a more realistic model and consider reactive power limitations, we propose the use of ac OPF, which is non-linear and non-convex and makes the problem further computationally expensive. Since the size of industrial electrical grids is large and the problem includes voltage/reactive power control settings, including binary variables to the ac OPF optimization problem will make it NP-Hard [46], [47] and much more computationally expensive. Therefore, instead of adding binary variables, we propose to solve the UC based on the energy prices in a way that the cheapest units become online until enough generation capacity is available to satisfy the load and losses in each hour.

B. Including Weather Data

Since the output power of renewable energy resources such as wind turbines and solar power plants is directly related to the weather conditions, weather information was directly included in the power flow modeling, per the strategy outlined and validated in our previous work [48], [49]. The

availability of weather information, the mapping of weather information to electric grid components, and a flexible and extensible modeling approach for relating weather values to the power flow models are introduced in this study. This strategy is applied to the time step simulation to find the output generation of renewable resources. In the next step, to find the optimal dispatch of conventional generators, considering reactive power limitations, an ac OPF is solved.

C. AC Optimal Power Flow

AC OPF [41] is used to find a steady-state result of a power system that minimizes the cost of real power generation, $\mathcal{F}_c(P_G)$, defined by coefficients a, b, and c, representing quadratic cost curve parameters of generators. The objective function can be represented as:

$$\min_{P_G} \mathcal{F}_c(P_G) = \sum_{g=1}^{|\mathcal{G}|} [a_g + b_g P_G, g + c_g P_G^2, g] \tag{1}$$

Solutions must satisfy the power balance equations (Eq. 2-3) and system operational constraints accounting for real and reactive power limits on generators (Eq. 4-5), bus voltage magnitude (Eq. 6), and thermal line limits (Eq. 7) [50].

$$P_{G,(g\in\mathcal{G}(i))} - P_{D,i} = |V_i| \sum_{k=1}^{|N|} |V_k| (G_{ik}^Y cos\theta_{ik} + B_{ik}^Y sin\theta_{ik}) \tag{2}$$

$$Q_{G,(g\in\mathcal{G}(i))} - Q_{D,i} = |V_i| \sum_{k=1}^{|N|} |V_k| (G_{ik}^Y sin\theta_{ik} - B_{ik}^Y cos\theta_{ik}) \tag{3}$$

$$P_{min,g} \leq P_{G,g} \leq P_{max,g} \qquad \forall g \in \mathcal{G} \tag{4}$$

$$Q_{min,g} \leq Q_{G,g} \leq Q_{max,g} \qquad \forall g \in \mathcal{G} \tag{5}$$

$$V_{min,i} \leq |V_i| \leq V_{max,i} \qquad \forall i \in N \tag{6}$$

$$P_e^2 + Q_e^2 \leq S_{max,e}^2 \qquad \forall e \in \mathcal{E} \tag{7}$$

In the equations, $|V_i|$ presents the voltage magnitude at the i^{th} bus, and θ_i variable is the voltage angle at the i^{th} bus. The θ_{ik} is the difference in voltage angles of the i^{th} and k^{th} buses. Here, N is the set of buses in the system. The real and reactive power demands at the i^{th} bus are represented as $P_{D,i}$ and $Q_{D,i}$, respectively. Real and reactive power generation of the g^{th} generator are represented as $P_{G,g}$ and $Q_{G,g}$. Note that $\mathcal{G}$ is the set of all generators in the system. The bus admittance matrix is represented in its real component as G_{ik}^Y, and B_{ik}^Y for its imaginary component. The generator minimum and maximum operating limits are provided as $(P_{min,g}, P_{max,g})$ for real power, and $(Q_{min,g}, Q_{max,g})$ for reactive power. Operating limits to the bus voltage magnitude are bounded by $(V_{min,i}, V_{max,i})$. The flow of power on each branch, e, is limited by its thermal limit, $S_{max,e}$, related to the flow of real and reactive power in Eq. 7, where the power flowing on each branch is given by the power flow equations (Eq. 8-9). Note that $\mathcal{E}$ is the set of all branches in the system.

$$P_e = |V_i|^2 G_{ik}^Y - |V_i||V_k|(G_{ik}^Y cos\theta_{ik} + B_{ik}^Y sin\theta_{ik}) \tag{8}$$

$$Q_e = -|V_i|^2 B_{ik}^Y - |V_i||V_k|(B_{ik}^Y cos\theta_{ik} - G_{ik}^Y sin\theta_{ik}) \tag{9}$$

IV. Calculating Operational Emissions

In this section, the main emissions from transportation that are harmful to human health and environment including CO_2, NO_x, $PM_{2.5}$, VOCs, and CO are studied [2], [51]. These emissions can be generated directly from ICE tailpipe, or indirectly from the power plants' increased generation to account for the EV charging load. The operational emissions may be compared across different scenarios. In scenarios in which EV load is modeled, the emissions impact is captured within the operational emissions calculated for the grid.

A. Grid Emissions

The emissions from power plants are calculated using the procedure introduced in [35]. This emissions calculation process uses the grid dispatch information of the scenario and pollutant rates provided by fuel type in the Greenhouse gases, Regulated Emissions, and Energy use in Transportation (GREET®) model [52]. The emission factors for common environmental pollutants are provided in Table II, with 2030 emission factors from coal, natural gas, and nuclear from [52] and petroleum coke from [53]. There are no operational emissions from renewable energy generation.

TABLE II:
2030 Generator Emission Factors (lb/MWh) by Fuel Type [52], [53]

Fuel Type	VOC	NO_x	$PM_{2.5}$	CO_2	CO
Coal	0.0059	0.45994	0.07575	406.87	0.04944
Natural Gas	0.0064	0.00853	0.00227	165.56	0.07439
Nuclear	0	0	0	0	0
Petroleum Coke	0.01156	2.9796	0.06218	2619.538	0.16296

The operational emissions of power plants in the electric grid are calculated using Eq. 10. The dispatch over the period of simulation provides the energy contribution from each generator, or E_G. The emissions factor (EF) corresponding to the fuel type of the generator is used. The product of these provide the operational emissions (OE) of a particular pollutant and a generator for the duration of the simulation. This process is repeated for each generator in the case and aggregated on a case-level by pollutant. Note that renewable generation including hydro, solar, and wind, have no associated operational emissions. This calculation is shown in Eq. 10 for the pollutant p, where $\mathcal{G}$ is the set of all generators in the system, and $EF_p(f_i)$ is the pollutant p emission factor of the i^{th} generator's fuel type (f_i).

$$OE_p = \sum_{i=1}^{|\mathcal{G}|} (E_{G_i} * EF_p(f_i)) \tag{10}$$

TABLE III:
ICE Emission Factors (g/mile)

	VOC	NO_x	$PM_{2.5}$	CO_2	CO
LD	0.005 [56]	0.05 [57]	0.007 [57]	404 [58]	2.2 [57]
MHD	0.033 [56]	1.31 [57]	0.033 [57]	1,766 [59]	5.9 [57]

B. Transportation Emissions

The emissions from traditional ICE vehicles are calculated based on the hourly miles traveled by LD and MHD EVs in a region during a sample day. This study adapts this approach to perform hourly calculations. Table III shows the average g/mile emissions from CO_2, NO_x, $PM_{2.5}$, VOCs, and CO for different EV types (LD and MHD) and their references. This table and the estimated amount of miles traveled in each hour [54] are used to perform hourly emission calculations for different vehicle types. Also, as explained in [55], a multiplier is used to scale the running emissions to total emissions as ICE cars and trucks can generate emissions when they start, idle, and park with their power on, in addition to when they are traveling. As it can be observed from Table III, CO_2, CO, and NO_x have higher emission rates and are mostly detrimental to the environment but according to Table I, a smaller amount of $PM_{2.5}$ and VOC are more dangerous for human health, so even small changes in $PM_{2.5}$ and VOC can be impactful.

V. Case Study

A. Electrical Grid Model

Since the actual grid data are considered to be critical energy infrastructure information (CEII) with restricted access for research, we have used U.S. Energy Information Association (EIA) generation data [60], and census data to approximate the load in our previous work [61]–[63] and created realistic synthetic grids, validated using the methodology in [64].

The electric grid used in this study is a synthetic network geographically sited in Texas, U.S., with around 7000 buses created based on actual generator data [31]. A diagram depicting the transmission lines in this synthetic grid is shown in Figure 2, with the teal lines representing transmission lines with a voltage level of 345 kV, black lines showing transmission lines with a voltage level of 138 kV, and green lines displaying transmission lines with a voltage of 69 kV. The synthetic Texas grid was originally created based on the EIA 860 form of 2019 generator data [60]. The electric grid models used for simulation in this case study represent updated versions of this case, representing the 2020 system, and a future 2030 system. The 2020 case contains the updated generation included in the 2020 release of the EIA 860 data, and the 2030 case was created based on proposed generation changes through 2023 including generator parameters and locations, and a Long-Term System Assessment (LTSA) report released from ERCOT including a long-term view of anticipated changes in the grid [32]. In the EIA 860 data set, the proposed changes in the generators up to 2023 are mentioned with details of generators' parameters and their proposed locations. In addition, the ERCOT presents a long-term view of the anticipated changes in the grid in a report called Long-Term System Assessment (LTSA) [32]. These data are used to upgrade the synthetic Texas grid based on the prediction by year 2030. The main changes by 2030 include the solar plants increase from 2,335 MW capacity in 2019 to 26,835 MW by 2030 with an increase by a factor of 11.5 and the wind turbines will have 30,000 MW increase by 2030 by a factor of 2.2. The number of generators with the natural gas fuel type also increases but the main part of added units include combined cycle power plants. Retirement is also predicted based on ERCOT LTSA and two coal units with an overall capacity of 1,441 MW are retired by 2030. This grid, which is available at [31] is then used for creating synthetic load at the bus level and mapping EV load to the closest buses. Table IV compares the generation capacities of the studied grid in 2020 and 2030 and Table V shows a comparison of important characteristics of the studied grids in 2020 and 2030.

TABLE IV:
Comparing Generation Capacity by Fuel Type for Synthetic Texas Grid Case in 2020 and 2030

	2020 Capacity (MW)	2030 Capacity (MW)	Difference
Solar	2,335	26,835	24,500
Wind	25,702	55,702	30,000
Natural Gas	56,539	62,434	5,895
Battery	0	1,603	1,603
Coal	14,407	12,966	-1,441

TABLE V:
Texas Synthetic Grid Overview in 2020 and 2030

	Value in 2020	Value in 2030
Number of buses	6,717	7,132
Number of substations	4,894	4,894
Number of areas	8	8
Number of transmission lines	7,168	7,223
Number of transformers	1,967	2,332
Number of phase shifters	2	2
Number of loads	4,856	5,095
Number of generators	731	1,058
Number of shunts	634	684

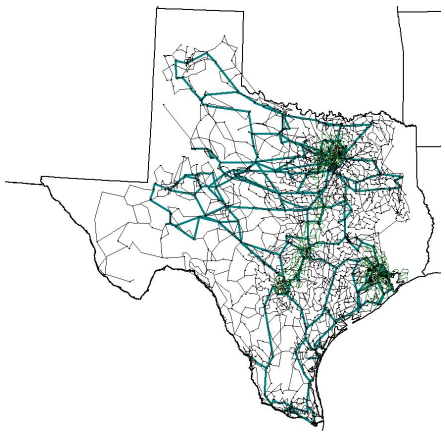

Fig. 2: Transmission lines in the synthetic Texas grid

B. Transportation Model

The transportation data contains the road data on geographical footprint of the greater Houston area, Texas, U.S., including Harris, Chambers, Galveston, Brazoria, Waller, Fort

TABLE VI:
Summary of Scenarios

	Scenario Name	Grid Model Year	Grid Loading	EV Penetration	Renewable Generation
1	2020 High Load Base Case	2020	High	0% LD, 0% MHD	Moderate Renewables
2	2020 High Load EV1	2020	High	20% LD, 10% MHD	Moderate Renewables
3	2020 High Load EV2	2020	High	30% LD, 20% MHD	Moderate Renewables
4	2020 Low Load Base Case	2020	Low	0% LD, 0% MHD	Moderate Renewables
5	2020 Low Load EV1	2020	Low	20% LD, 10% MHD	Moderate Renewables
6	2020 Low Load EV2	2020	Low	30% LD, 20% MHD	Moderate Renewables
7	2030 High Wind Base Case	2030	High	0% LD, 0% MHD	High Wind
8	2030 High Wind EV1	2030	High	20% LD, 10% MHD	High Wind
9	2030 Low Wind Base Case	2030	High	0% LD, 0% MHD	Low Wind
10	2030 Low Wind EV1	2030	High	20% LD, 10% MHD	Low Wind

Bend, and Montgomery counties. The EV charging scenarios presented in this paper were set up to mimic the natural charging behaviors of drivers and fleets. That is, based on behaviorally-aware surveys, we assume that drivers prefer to charge at home as soon as they arrive home. Similarly, fleet vehicles charge as soon as they arrive at their depots. Thus, most of the LD EV chargers are represented in residential areas and the MHD EV chargers are represented at depot locations. Figure 3 shows the added demand from the LD and MHD EV charging. Most of the LD EV demand occurs at home overnight, coincidentally during the power grid's off-peak hours. However, since MHD EVs are mostly used for business, the charging pattern of MHD EVs is flatter with a minor increase at 7:00 PM which is close to peak load time. Based on predictions for the level of EV integration by 2030 [65], the scenarios studied represent 20% integration of LD vehicles and 10% integration MHD vehicles integrated and a scenario with no transportation electrification.

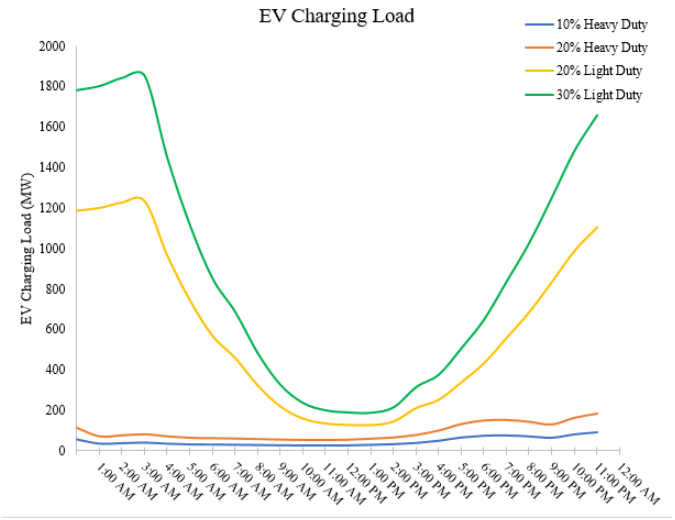

Fig. 3: The LD and MHD EV charging load for the greater Houston region over a 24-hour period

C. Simulation Scenarios

The case study presents hourly simulation for ten simulation scenarios to demonstrate the performance of the comprehensive, realistic, and implementable strategy of calculating spatiotemporal operational emissions proposed in this paper, summarized in Table VI. The 2020 Texas synthetic case is used to demonstrate the method strategy in grid conditions of low and high loads, and two different EV penetrations. The 2030 Texas synthetic case is used to demonstrate the strategies with low and high levels of wind generation availability.

System loads that are not related to EV charging were created for the sample day for the case using the approach outlined in [40]. The grid loading is rated high in both weather cases in 2030. Note that the load in 2030 will grow by 20% compared to the load in 2020 based on [32]. The EV penetrations levels simulated include the following:

1) **Base Case**: No transportation electrification included
2) **EV1**: 20% LD and 10% MHD transportation electrification in the greater Houston area
3) **EV2**: 30% LD and 20% MHD transportation electrification in the greater Houston area

The aggregate time series of EV and power system loads are shown during the selected 24-hour period of simulation in Figure 4. The hourly renewable generation time series was created leveraging real weather data from the same day and using speed-power curves to translate the wind speed from

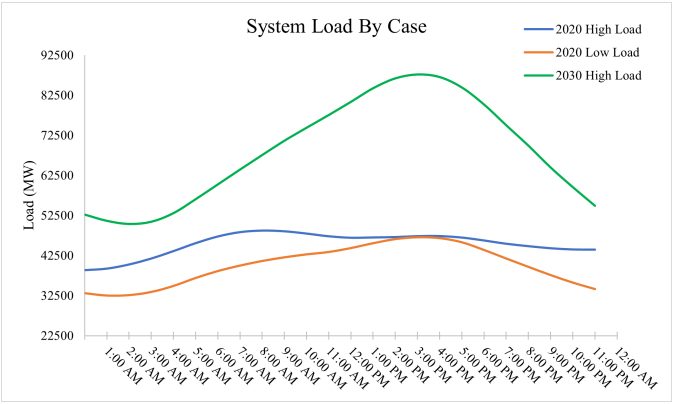

Fig. 4: System load time series for 2020 High Load, 2020 Low Load, and 2030 High Load synthetic Texas grid cases

the weather data to the power generated by the wind turbines, and cloud coverage to solar cells as demonstrated in [48] and validated in [49].

For each scenario, the proposed UC and ac OPF are solved for every hour within the 24-hour period of simulation to calculate the hourly optimal output of each generator. Using the methods discussed in Section IV, the operational hourly emissions of each scenario are calculated and compared to

those of its respective base case (case of the same conditions without any transportation electrification).

D. Case Validation

The simulation scenarios are built from real data and validated models including real generator locations and parameters [60], real travel demand data [33], validated synthetic electric grid models, validated bus-level grid loads, validated weather-informed capacity of renewable generators. The validation of the grid models, grid loads, and weather-informed renewable generation capacity compared the performance of these models to real data, as described below.

The synthetic electric grid models used in the scenarios have been validated according to [64]. This metric-based validation process evaluated the realism of synthetic electric grid models relative to real industrial grid models. The model was evaluated across eighteen validation metrics including the number of buses per substation, the percentage of substations containing buses in voltage ranges, the percentages of substations that contain loads, the load per bus, the ratio of generation capacity to load, the number of substations with generators, the capacities of the generators, the ratio of maximum reactive and maximum real power of generators, transformer reactance, ratio of transformer reactance and resistance, lines per substation, lines on a minimum spanning tree, distance of a line along a Delaunay triangulation, and total line length. The bus-level grid loads of each scenario have been validated according to [40]. The synthetic bus-level loads were compared to real data from electric grids and have been validated according to metrics including the load factor, load distribution curves, autocorrelation of load time series, and power spectral densities. Also, the performance of the weather-informed calculation of renewable generators' capacities used in setting the renewable generation capacity of each scenario is documented in [49], in which the calculated generation capacity is compared to recorded dispatch of renewable generators in areas of the United States.

VI. Simulation Results

The results show the operational emissions for the electrification of the transportation network of the greater Houston area and the 7000-bus electric grid on the footprint of Texas for each scenario discussed in Section V. The electric grid's operational emissions are determined by the dispatch of generators with different fuel types, so the hourly generation dispatch is presented by fuel type over each 24-hour period. Results include total emissions of VOC, NO_x, $PM_{2.5}$, CO_2, and CO over the 24-hour period from each sector as well as temporal and spatial representations of the differences between the scenarios and their respective base cases. The results are discussed in Section VII.

A. Transportation Operational Emissions

Reference [55] shows the average miles traveled per mile in Houston that are used to calculate the overall emissions of the vehicles for a day. These values were then converted to standard units and are displayed in Table VII. The combined LD and MHD results are presented in Table VIII.

B. Generator Dispatch by Fuel Type

Figure 5 presents the grid's dispatch of generators by fuel type in the base case (no EV integration). Figure 6 presents the difference in generation dispatch by fuel type when comparing the EV scenario to the base case.

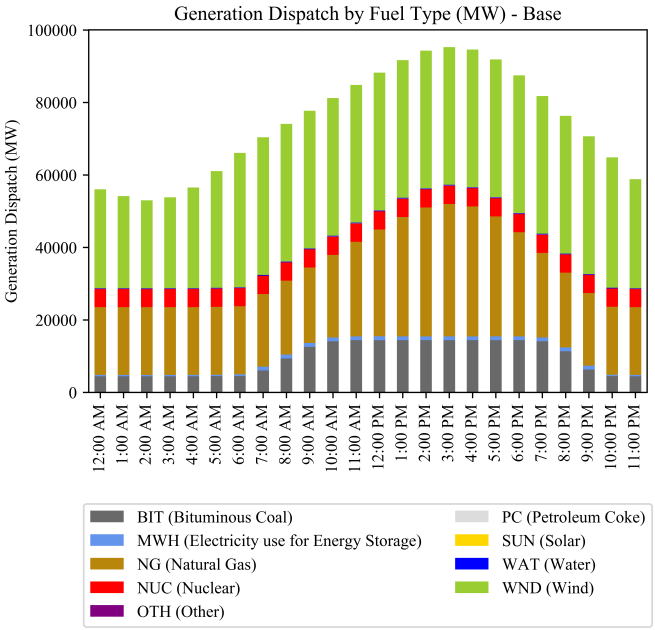

Fig. 5: Dispatch of Grid Generators by Fuel Type for the 2030 High Wind Base Case (MW)

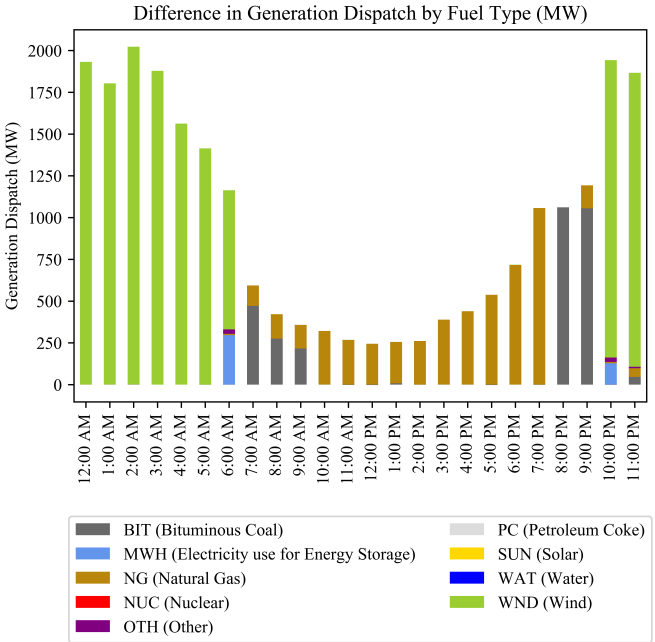

Fig. 6: Difference in Dispatch of Grid Generators in 2030 High Wind Case by Fuel Type (MW)

TABLE VII:
Greater Houston Area ICE Emissions by LD and MHD Vehicles (lb)

		VOC	NO_x	$PM_{2.5}$	CO_2	CO
Base Case	LD ICE	2,795	24,659	3,836	221,384,752	1,208,300
	MHD ICE	2,248	89,459	2,248	120,104,311	402,397
EV1	LD Difference	-559	-4,932	-767	-44,276,950	-241,660
	MHD Difference	-225	-8,946	-225	-12,010,435	-40,240
EV2	LD Difference	-839	-7,398	-1,151	-66,415,425	-362,490
	MHD Difference	-450	-17,892	-450	-24,020,870	-80,480

TABLE VIII:
Operational Emissions of the Greater Houston Area's Transportation (lb)

		VOC	NO_x	$PM_{2.5}$	CO_2	CO
	Base Case	5,043	114,119	6,084	236,074,747	1,610,697
	EV1	4,259	100,241	5,092	285,201,678	1,328,797
	EV2	3,754	88,828	4,483	251,052,768	1,167,727
EV1	Difference (lb)	-784	-13,878	-992	-56,287,385	-281,900
	Difference (%)	-15.55	-12.16	-16.31	-16.48	-17.50
EV2	Difference (lb)	-1,289	-25,290	-1,601	-90,436,295	-442,970
	Difference (%)	-25.56	-22.16	-26.31	-26.48	-27.50

TABLE IX:
Operational Emissions of the Grid's Generators (lb)

			VOC	NO_x	$PM_{2.5}$	CO_2	CO
2020 High Load Case		Base Case	5,029	178,601	23,282	204,932,620	53,169
		EV1	5,534	185,972	23,576	218,490,155	59,054
		EV2	5,029	178,603	23,282	204,936,148	53,170
	EV1	Difference (lb)	505	7,371	294	13,557,535	5,885
		Difference (%)	10.04	4.13	1.26	6.62	11.07
	EV2	Difference (lb)	0	2	0	3,528	1
		Difference (%)	0.00	0.00	0.00	0.00	0.00
2020 Low Load Case		Base Case	4,450	161,486	21,267	183,637,023	46,875
		EV1	4,450	161,487	21,267	183,636,780	46,874
		EV2	4,450	161,487	21,267	183,636,744	46,874
	EV1	Difference (lb)	0	1	0	-243	-1
		Difference (%)	0.00	0.00	0.00	0.00	0.00
	EV2	Difference (lb)	0	1	0	-279	-1
		Difference (%)	0.00	0.00	0.00	0.00	0.00
2030 High Wind Case		Base Case	5,012	156,980	18,728	190,647,824	54,227
		EV1	5,063	158,853	18,977	192,763,928	54,761
	EV1	Difference (lb)	51	1,873	249	2,116,104	534
		Difference (%)	1.01	1.19	1.33	1.11	0.98
2030 Low Wind Case		Base Case	5,152	163,469	19,630	197,393,681	55,641
		EV1	5,152	163,469	19,630	197,393,895	55,641
	EV1	Difference (lb)	0	0	0	214	0
		Difference (%)	0.00	0.00	0.00	0.00	0.00

C. Grid Operational Emissions

Table IX presents the operational emissions from the electric grid for both scenarios. Emissions from the grid are observed to increase by between 0% and 11% for each pollutant (most by either 0% or 1%) when considering the additional demand from the EV scenario compared to the base case.

D. Combined Operational Emissions

The combined operational emissions of the electrical grid and transportation network are presented in Table X. For a more detailed study, we select the 2030 high-wind case with EV1 penetration levels to take a closer look at the spatiotemporal resolution of the combined operational emissions. Considering the temporal characteristics of operational emissions provides useful context for understanding their impacts. Figures 7 and 8 present the hourly difference in dispatch comparing the EV scenario to the base case. Hours of interest within this case include 6:00 AM, 5:00 PM, and 9:00 PM because they present the greatest percentage reduction in emissions, the greatest absolute reduction in emissions, and an increase in some emissions, respectively that are coincident with human outdoor activity.

Further information can be achieved by considering the locations where the emissions occurred during the noted hours of interest. Figures 9a, 9b, and 9c show the spatial distribution of emission changes with the incorporation of EV charging at 5:00 PM. Figures 10a, 10b, and 10c show the spatial distribution of emission changes with the incorporation of EV charging at 9:00 PM and Figures 11a, 11b, and 11c show the overall differences in NO_x, $PM_{2.5}$ and VOC operational emissions, from the entire 24-hour simulation period, respectively. In these Figures, each circle represents changes in the emissions from the grid or transportation and the area of circles are proportional to the amount of emissions for that time step. The scales vary for legibility and are indicated in the figure

TABLE X:
Combined Operational Emissions of the Grid's Generators and the Greater Houston Area's Transportation (lb)

			VOC	NO_x	$PM_{2.5}$	CO_2	CO
2020 High Load Case		Base Case	10,072	292,719	29,366	558,940,752	1,663,866
		EV1	9,793	286,213	28,668	514,958,999	1,387,852
		EV2	8,784	267,432	27,766	466,004,179	1,220,898
	EV1	Difference (lb)	-279	-6,507	-698	-43,981,753	-276,014
		Difference (%)	-2.77	-2.22	-2.38	-7.87	-16.59
	EV2	Difference (lb)	-1,288	-25,287	-1,600	-92,936,573	-442,968
		Difference (%)	-12.79	-8.64	-5.44	-16.63	-26.62
2020 Low Load Case		Base Case	9,493	275,604	27,351	537,645,155	1,657,572
		EV1	8,709	261,727	26,360	480,105,624	1,375,671
		EV2	8,205	250,315	25,751	444,704,775	1,214,602
	EV1	Difference (lb)	-784	-13,877	-992	-57,539,531	-281,900
		Difference (%)	-8.26	-5.04	-3.63	-10.70	-17.01
	EV2	Difference (lb)	-1,288	-25,289	-1,600	-92,940,381	-442,970
		Difference (%)	-13.57	-9.18	-5.85	-17.29	-26.72
2030 High Wind Case		Base Case	10,055	271,098	24,812	426,722,571	1,664,924
		EV1	9,322	259,094	24,094	383,092,725	1,383,558
	EV1	Difference (lb)	-733	-12,004	-743	-43,629,846	-281,366
		Difference (%)	-7.29	-4.43	-3.00	-10.22	-16.90
2030 Low Wind Case		Base Case	10,195	277,587	25,714	551,401,813	1,666,338
		EV1	9,411	263,710	24,722	493,862,739	1,384,438
	EV1	Difference (lb)	-784	-13,877	-992	-57,539,075	-281,900
		Difference (%)	-7.69	-5.00	-3.86	-10.44	-16.92

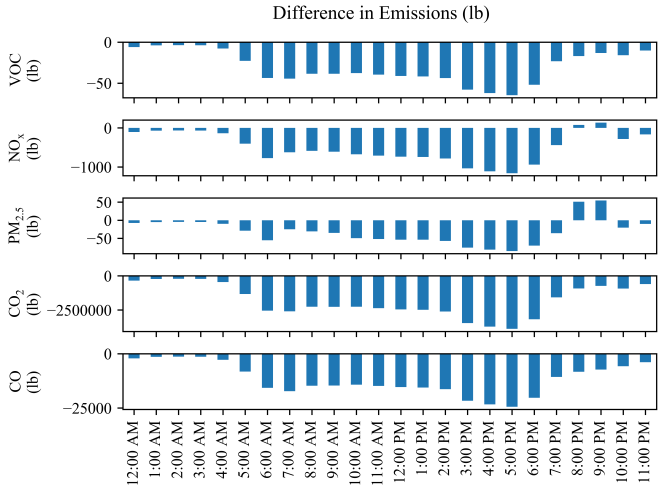

Fig. 7: Hourly difference in emissions between EV and base scenarios (lb)

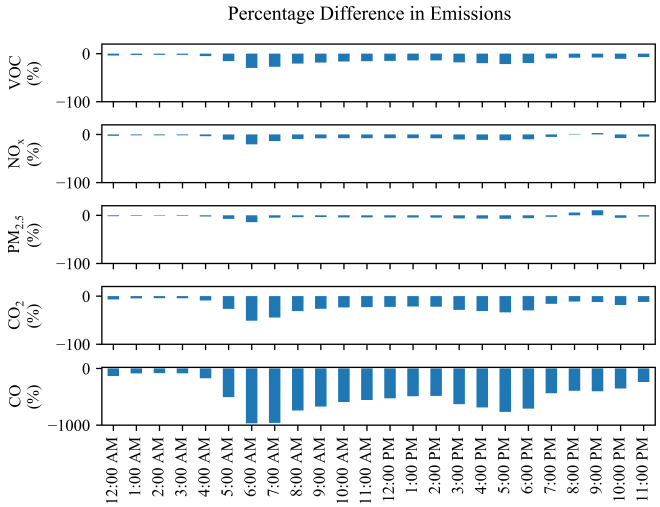

Fig. 8: Hourly percentage difference in emissions between EV and base scenarios (%)

captions in relation to the combined transportation emissions. Exact locations are slightly shifted to enable better visibility of overlapping circles. The color of the circles represents an increase (red) or decrease (green) in emissions. Since at 6:00 AM there is almost a pure reduction in the emissions by considering EV scenario and red circles were barely visible, those figures are not shown.

VII. Discussion

A variety scenarios are studied and compared in this section. Comparing 2020 high load and low load scenarios, it is observed that as the electrical demand is increased in the base case (ignoring the impact of EVs), more power is needed from conventional generators (e.g., generators with natural gas or coal fuel) since renewable resources basically use free resources and are used to the maximum extent allowed by the available resources. These conventional generators, also called "peakers" (meaning are mostly used for peak loads), are creating more harmful emissions. Therefore, the advantage of adding EVs in the low load case is that the difference between the base load and EV charging load is mostly satisfied with renewable resources. However, replacing specific percentages of ICE cars with EVs reduces overall daily emissions of all pollutants for both studied load scenarios in 2020.

Overall, this study shows a reduction in operational emissions with the electrification of transportation. Table X presents the combined operational emissions from the grid and the transportation networks. The electrification 20% of Houston's LD vehicles and 10% of its MHD vehicles yields approximately 19,790 metric tons (10%) daily reduction in CO_2 emissions, and nearly 128 metric tons daily (17%) reduction in

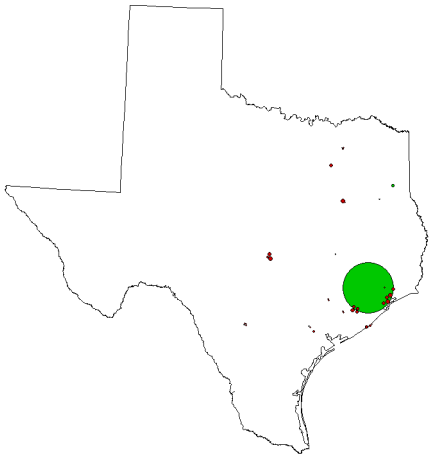

(a) NO_x difference in transportation emissions: -1204 lb.

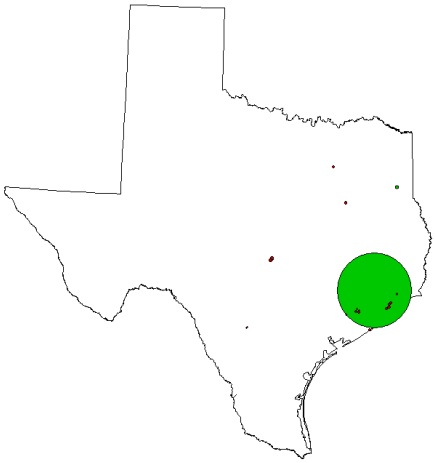

(b) $PM_{2.5}$ difference in transportation emissions: -86 lb.

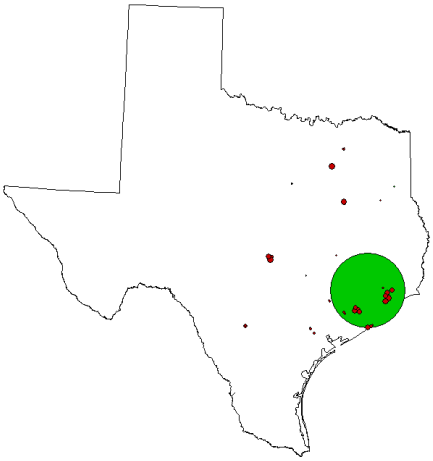

(c) VOC difference in transportation emissions: -68 lb.

Fig. 9: Spatial distribution of difference in operational emissions at 5:00 PM
(green: decreases with EVs, red: increases with EVs).

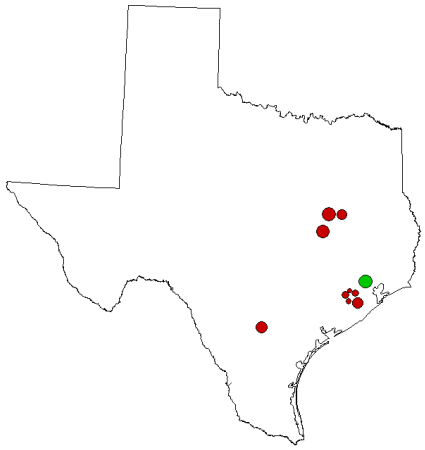

(a) NO_x difference in transportation emissions: -360 lb.

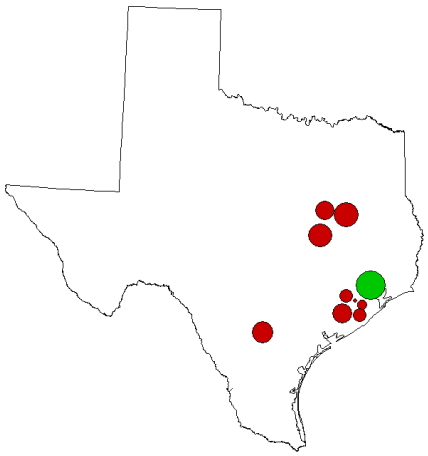

(b) $PM_{2.5}$ difference in transportation emissions: -26 lb.

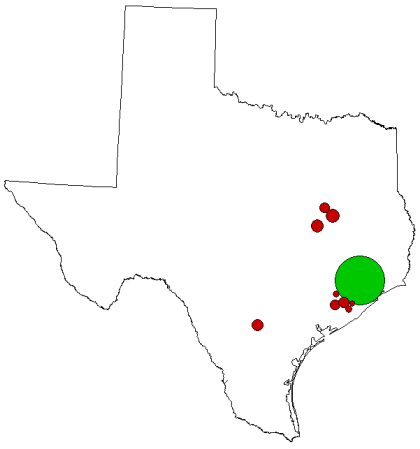

(c) VOC difference in transportation emissions: -20 lb.

Fig. 10: Spatial distribution of difference in operational emissions at 9:00 PM
(green: decreases with EVs, red: increases with EVs).

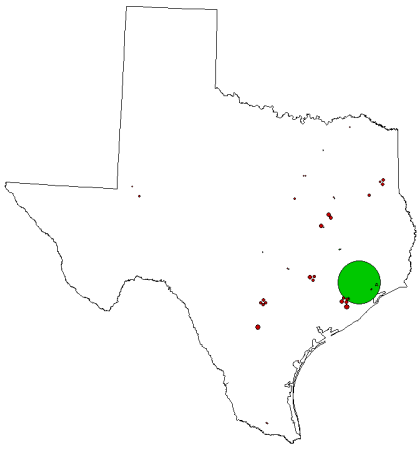

(a) NO_x difference in transportation emissions: -13,878 lb.

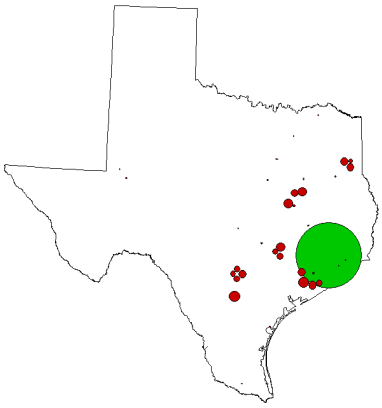

(b) $PM_{2.5}$ difference in transportation emissions: -992 lb.

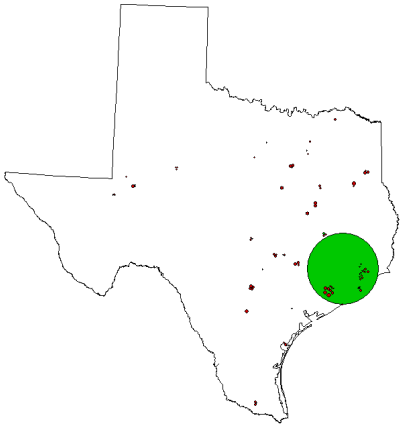

(c) VOC difference in transportation emissions: -784 lb.

Fig. 11: Spatial distribution of cumulative difference in operational emissions over the 24-hour period (green: decreases with EVs, red: increases with EVs).

CO emissions for the day studied. The effect of emission from CO and CO_2 is cumulative [3], so these emissions reductions over the total period of simulation are meaningful. Overall, the reduction in the emissions is attributed to reducing the operational emissions of transportation (as seen in Table VIII). Instead, small increases in the grid emissions were observed (see Table IX). The scale of the transportation emissions reductions in the EV scenario (-12% to -19%) was larger than that of the grid emissions increase (+1%), thus the net operational emissions reductions is observed (-3% to -17%).

A. Generator Dispatch by Fuel Type

Figure 5 presents the grid's dispatch of generators by fuel type in the base case (no EV integration). Because the weather in the studied case presents a windy and cloudy day, wind accounts for a large portion of the generation mix and solar is not present in the generation mix. The availability of renewable generation resources is weather-dependent. Had there been fewer clouds, the solar availability would have been nonzero and would have been present in the generation mix. Since there are no operational costs associated with renewable generation, the generation from renewable resources is dispatched to the maximum extent allowed by the transmission network. As there are no operational emissions associated with renewable generation, the weather in the simulation impacts the operational emissions of the generation from the grid. Therefore, during hours with lower wind and solar availability, conventional power plants account more for the generation and thus produce the associated emissions. This shows the importance of including weather data in the OPF input problem when evaluating operational emissions. However, there are operational emissions associated with conventional generation (see Table II). The contribution from nuclear plants is relatively constant across the hours of simulation, consistent with its typical dispatch. The coal and nuclear generators' dispatch follows load patterns, with light coal dispatch in the nighttime hours due to its cost relative to that of wind power. The greater wind availability in the overnight hours provides greater wind power generation capacity.

Figure 6 presents the difference in generation dispatch by fuel type when comparing the EV scenario to the base case. Since the load is higher at all hours in the EV scenario, the differences in Figure 6 are largely positive. Increased use of wind generation accounts for much of dispatch changes observed in the nighttime hours, coincident with the hours of peak LD EV demand. The EV demand at 6:00 AM is served by a combination of wind generators and energy storage. The EV demand from 7:00 AM to 9:00 AM is served by a combination of coal and natural gas. The daytime EV demand was largely served by natural gas generators. The daytime use of conventional generation to serve the added EV demand within the system is attributed to the cheaper generation (renewables and nuclear) already being dispatched maximally within the base case. The EV demand at 8:00 PM is served by coal generation. The sudden change between the generator fuel type serving the 7:00 PM and 8:00 PM EV demand is attributed to the coal generation being dispatched maximally

in the base case and the dispatch in the EV case from the late morning to 7:00 PM, so the dispatch of generation serving the added EV demand is purely natural gas for these hours. The load and coal dispatch in the base case decreases at 8:00 PM and thus coal capacity will be available to serve the EV demand at 8:00 PM with less cost than natural gas. The EV demand at 10:00 PM is served by a combination of wind generators and energy storage.

Given that coal generation supplies EV demand at 8:00 PM and 9:00 PM, which results in higher emissions, design of smart charging strategies and pricing incentives to encourage drivers and fleets to charge outside those hours, especially in off-peak hours will be highly beneficial.

B. Temporal and Spatial Operational Emissions

The overall combined operational emissions of the electrical transmission grid and transportation networks of Houston are presented in Table X. Since the temporal and spatial distributions of specific pollutants determine the risk factor for humans' health, the distributions of these pollutants are studied in this paper. Considering the temporal characteristics of operational emissions provides useful context for understanding their impacts. For example, it is advantageous to the environment and human health if particular pollutants such as VOC, $PM_{2.5}$, and NO_x are reduced during periods of outdoor human activity, such as the morning when people are beginning their day and the evening when people are beginning post-school and post-work activities. Outdoor human activity exposes people to the pollutants outside their homes. Additionally, these pollutants in the presence of UV radiation contribute to O_3 creation which presents a hazard to human respiratory health [8], so emissions associated with the production of O_3 should be minimized during daylight hours for optimal human health outcomes.

Figures 7 and 8 present the hourly difference in dispatch comparing the EV scenario to the base case. The greatest absolute reduction of emissions occurred during the afternoon hours across all emissions studied (Figure 7) whereas the greatest percentage reduction occurred around 6:00 AM as desired (see Figure 8). The $PM_{2.5}$ and NO_x increased in the EV scenario relative to the base scenario at 8:00 PM and 9:00 PM due to the change in the generation of increased demand from EVs from natural gas to coal which is cheaper but based on Table II has more contribution in the creation of harmful emissions.

From 12:00 AM to 6:00 PM when wind was available to supply the charging demand from EVs, the difference in grid emissions between the two scenarios was trivial, so the dominant difference in emissions between the two scenarios is attributed to the differences in the transportation emissions. The morning hours showed an overall reduction in emissions by nearly 30% for VOC, 20% for NO_x, 14% for $PM_{2.5}$, and approximately 970% for CO.

The evening hours of interest (5:00 PM and 9:00 PM) demonstrate larger changes in the emissions from the electric grid between the two scenarios. These changes are represented in Figures 9a-10c. At 5:00 PM, the NO_x emissions are reduced cumulatively by 12%. In the city of Houston, the emissions are reduced by over 1200 lb from transportation alone (Fig. 9a). The emissions from the electric power grid's generators present smaller increases in NO_x emissions. Notably, some of these small increases occur on the outskirts of Houston and Austin, both with relatively high population densities. Other associated increased emissions from the power grid take place in sparsely-populated areas. At 5:00 PM, cumulatively $PM_{2.5}$ emissions are reduced by over 7% with similar spatial relationships observed, but in even smaller quantities (Fig. 9b). Here, the emissions from the transportation sector are reduced in Houston by 86 lb, with the changes observed due to the electric grid generation being substantially less. VOC emissions at 5:00 PM experience a reduction of approximately 20%. Figure 9c shows the spatial distribution of these changes, with the reduction from the transportation sector accounting for 68 lb. Here, some of the small increases in power plant emissions occur in Houston, Austin, and Dallas, though in much smaller amounts than the reduction in transportation emissions.

At 9:00 PM, some of the emissions are increased in the EV scenario relative to the base scenario. For example, $PM_{2.5}$ emissions increased by 10% and NO_x emissions increased by about 3%. Because these increases coincide with a time past sunset, the creation of O_3 and since human outdoor activity is relatively low at 9:00 PM, direct exposure to these emissions is less of a concern. The spatial distributions of emissions with a net increase (NO_x and $PM_{2.5}$) are shown in Figures 10a and 10b, where the emissions reductions from the transportation sector are 360 lb and 26 lb, respectively. The increase in emissions is attributed to the same set of generators in slightly different proportions. Two of the three clusters of increased power plant emissions occur in rural areas south of San Antonio and Dallas. The third cluster of increased power plant emissions occurs in the southern portion of the greater Houston area. This hour and the preceding are notably the only hours for which any increase in combined operational emissions is observed. This is because the demand from EV scenario is being predominantly supplied by coal with relatively higher rates of emission for NO_x and $PM_{2.5}$. All other emissions are reduced at this hour. For example, the spatial distribution of VOC emissions is shown in Figure 10c. Here, the reduction in emissions from the transportation sector is 20 lb. The corresponding increase from the electric grid occurs in the same locations noted for NO_x and $PM_{2.5}$, but in relatively smaller magnitudes.

C. Sensitivity Analysis

The proposed strategy is adaptable to a variety of input conditions, a range of which are studied in this paper. By comparing extreme scenarios, ranges of possible emissions for a specific grid and transportation data can be estimated. A sensitivity analysis was conducted to quantify the sensitivity of the results for specific grid data and transportation data. The sensitivity of the operational emission results to grid load level variations show that VOC emissions were the most sensitive to load variations for EV1, followed by NO_x, $PM_{2.5}$,

and CO_2. CO emissions were not sensitive to changes in the grid conditions, as it changed by less than 1% for both EV1 and EV2 comparisons of high and low load scenarios. $PM_{2.5}$ was the most sensitive pollutant to load level changes in EV2, followed by VOC, NO_x, and CO_2. Based on the sensitivity results, CO_2 was the most sensitive to wind levels, with a 22% difference in CO_2 emissions was observed when comparing the high and low wind scenarios. The remaining pollutants were less sensitive (less than 3% change) to differences in wind conditions. These sensitivity analyses can be used to bound expectations of results for each pollutant in the extremes of grid, weather, and EV penetration conditions.

VIII. Conclusions

This paper proposes a strategy for obtaining realistic calculations of spatiotemporal operational emissions from coupled transportation and power grid sectors. The realism of the results can be attributed to the scale, realism, and geographic consistency of the data and models. The transportation networks rely on actual transportation data, travel patterns, traffic models, and behavior-informed simulations of LD and MHD charging. This methodology can be applied to any power grid model that includes geographic data and generator cost and fuel type information. This framework enables the evaluation of the impact of electrifying transportation on the combined operational emissions of the transportation network and the electric power grid. The studied pollutants include CO_2, NO_x, $PM_{2.5}$, VOC, and CO due to their prevalence in the transportation sector as well as concerns related to environmental and human health. The impacts of the spatiotemporal operational emissions are also discussed.

The study was performed using a 7000-bus synthetic electric grid on the footprint of Texas so as not to compromise any CEII, created based on publicly available data of actual generators in 2020 and validated to be structurally and functionally similar to the actual grid. Then, the grid is updated to reflect the predicted generation mix in 2030. The study compared a base case without EV integration to a case that replaces a variety of possible penetration levels of LD and MHD ICE vehicles with EVs in the greater Houston area. The studied days include a variety of high/low load, and high/low wind availability in 2020 and 2030 based on electrical grid and demand changes and simulation includes ac OPF with unit commitment and considers the impact of weather data directly in the calculations.

The results show a cumulative reduction in emissions by up to 40,000 metric tons (17%) of CO_2 emissions and up to 200 metric tons (27%) in CO emissions over the studied scenarios. Overall, the changes from the transportation sector yielded heavier influence than the changes in the electric grid. The predicted LD EV charging pattern employs mostly overnight off-peak hours which is coincident with lower demand from the overall load in the system and higher wind power availability, yielding lower operational emissions resulting from the EV charging demand. Also, authors show the importance of including weather in the ac OPF equations for emission calculations as it impacts the availability of renewable generation which is strongly related to the generation dispatch and resulting emissions of the grid.

The evaluation of emissions with temporal and local impact, i.e., NO_x, $PM_{2.5}$, and VOC, on a spatiotemporal basis provided valuable insights into the health and environmental impact of these emissions. The time of day and locations where these emissions are present can help evaluate to what extent people come into contact with the emissions. Periods of human outdoor activity (before and after work or school) in densely-populated areas are conditions for the locally-impacting emissions to have the greatest impact on human health outcomes. The time of day of emissions is also considered with respect to UV intensity, which can result in the production of O_3, associated with ecological and human health risks.

The methodology presented in this paper quantifies the spatiotemporal emissions of the electrification of ground transportation inclusive of ICE tailpipe emissions and grid emissions attributed to EV charging demand. This framework can be applied to grid and transportation networks in other locations, or could be used to study the emissions associated with different EV charging behaviors, penetration levels, or various weather and electric grid load scenarios. As transportation electrification is an important mechanism for reaching the goals set by emission reduction policies, this methodology could track the net progress made by such policy initiatives. Beyond evaluating if a strategy is meeting policy goals, calculating emissions with spatiotemporal resolution enables an understanding of the equity in the health and environmental impacts. This is aligned with the Justice40 Initiative [66] as it can ensure that the emissions of one area are not causing a detrimental increase in emissions in other areas, particularly those with disadvantaged communities. This is enabled by the spatiotemporal calculation of emissions and by the applicability of this methodology to large, industry-scale cases. In the future, this framework could additionally evaluate larger battery sizes of MHD EVs and smart charging schemes in which EV demand would be coordinated to reduce operational emissions or costs and perform experimental validation.

Acknowledgment

This work is partially supported through funding provided by the U.S. National Science Foundation (NSF) in Award 1916142, the U.S. Department of Energy (DOE) under award DE-OE0000895,U.S. DOE EERE Grant No. DE-EE0009665, the U.S. ARPA-E Grant No. DE-AR0001366, and the Power Systems Engineering Research Center (PSERC).

References

[1] M. Mazzarino, "The economics of the greenhouse effect: evaluating the climate change impact due to the transport sector in Italy," *Energy Policy*, vol. 28, no. 13, pp. 957–966, 2000.

[2] Y. Xu, F. E. Gbologah, D.-Y. Lee, H. Liu, M. O. Rodgers, and R. L. Guensler, "Assessment of alternative fuel and powertrain transit bus options using real-world operations data: Life-cycle fuel and emissions modeling," *Applied energy*, vol. 154, pp. 143–159, 2015.

[3] M. M. Klufallah, M. F. Nuruddin, M. F. Khamidi, and N. Jamaludin, "Assessment of carbon emission reduction for buildings projects in malaysia-a comparative analysis," in *E3S web of conferences*, vol. 3. EDP Sciences, 2014, p. 01016.

[4] D. Stevenson, F. Dentener, M. Schultz, K. Ellingsen, T. Van Noije, O. Wild, G. Zeng, M. Amann, C. Atherton, N. Bell *et al.*, "Multimodel ensemble simulations of present-day and near-future tropospheric ozone," *Journal of Geophysical Research: Atmospheres*, vol. 111, no. D8, 2006.

[5] A. García-Reynoso, A. Jazcilevich, L. Ruiz-Suárez, R. TORRES-JARDÓN, M. Suárez Lastra, and N. Reséndiz Juárez, "Ozone weekend effect analysis in México City," *Atmósfera*, vol. 22, no. 3, pp. 281–297, 2009.

[6] S. E. Pusede, A. L. Steiner, and R. C. Cohen, "Temperature and recent trends in the chemistry of continental surface ozone," *Chemical reviews*, vol. 115, no. 10, pp. 3898–3918, 2015.

[7] "Ecosystem Effects of Ozone Pollution". [Online]. Available: https://www.epa.gov/ground-level-ozone-pollution/ecosystem-effects-ozone-pollution

[8] "Health Effects of Ozone Pollution". [Online]. Available: https://www.epa.gov/ground-level-ozone-pollution/health-effects-ozone-pollution

[9] R. Newell, "Federal climate policy 101: Reducing emissions," 2021.

[10] "Volatile Organic Compounds ". [Online]. Available: https://www7.nau.edu/itep/main/eeop/docs/airqlty/AkIAQ_VolatileOrganicCompounds.pdf

[11] "NJ Hazardous Substance Fact Sheet ". [Online]. Available: https://nj.gov/health/eoh/rtkweb/documents/fs/1357.pdf

[12] "air hygiene ". [Online]. Available: https://www.indoorairhygiene.org/pm2-5-explained/#:$\sim$:text=Most%20studies%20indicate%20PM2.,breathing%20issues%20such%20as%20asthma.

[13] Carbon Dioxide Health Hazard Information Sheet . [Online]. Available: https://www.fsis.usda.gov/sites/default/files/media_file/2020-08/Carbon-Dioxide.pdf

[14] Carbon Monoxide Levels Chart . [Online]. Available: https://gaslab.com/blogs/articles/carbon-monoxide-levels-chart#:$\sim$:text=The%20OSHA%20personal%20exposure%20limit,an%208%2Dhour%20time%20period

[15] "Permissible Exposure Limits". [Online]. Available: https://www.osha.gov/annotated-pels/table-z-1

[16] S. P. Holland, E. T. Mansur, N. Z. Muller, and A. J. Yates, "The environmental benefits of transportation electrification: Urban buses," *Energy policy*, vol. 148, p. 111921, 2021.

[17] D. McCollum, V. Krey, P. Kolp, Y. Nagai, and K. Riahi, "Transport electrification: A key element for energy system transformation and climate stabilization," *Climatic change*, vol. 123, no. 3, pp. 651–664, 2014.

[18] K. Tartaglia, A. Birky, M. Laughlin, R. Price, and Z. Lin, "Transportation electrification beyond light duty: Technology and market assessment," Oak Ridge National Lab.(ORNL), Oak Ridge, TN (United States), Tech. Rep., 2017.

[19] K. L. Fleming, A. L. Brown, L. Fulton, and M. Miller, "Electrification of medium-and heavy-duty ground transportation: Status report," *Current Sustainable/Renewable Energy Reports*, vol. 8, no. 3, pp. 180–188, 2021.

[20] K. M. Bush, "Examining perceptions and priorities of heavy-duty transportation electrification projects: How considerations of justice can improve project implementation in environmental justice communities," Ph.D. dissertation, University of California, Davis, 2021.

[21] F. Orsi, M. Muratori, M. Rocco, E. Colombo, and G. Rizzoni, "A multi-dimensional well-to-wheels analysis of passenger vehicles in different regions: Primary energy consumption, co2 emissions, and economic cost," *Applied energy*, vol. 169, pp. 197–209, 2016.

[22] J. Woo, H. Choi, and J. Ahn, "Well-to-wheel analysis of greenhouse gas emissions for electric vehicles based on electricity generation mix: A global perspective," *Transportation Research Part D: Transport and Environment*, vol. 51, pp. 340–350, 2017.

[23] W. Ke, S. Zhang, X. He, Y. Wu, and J. Hao, "Well-to-wheels energy consumption and emissions of electric vehicles: Mid-term implications from real-world features and air pollution control progress," *Applied Energy*, vol. 188, pp. 367–377, 2017.

[24] I. Miller, M. Arbabzadeh, and E. Gençer, "Hourly power grid variations, electric vehicle charging patterns, and operating emissions," *Environmental Science & Technology*, vol. 54, no. 24, pp. 16 071–16 085, 2020.

[25] "Global car sales estimates". [Online]. Available: https://canalys.com/newsroom/canalys-global-electric-vehicle-sales-2020

[26] "Advanced Clean Cars II Regulations Resolution 22-12". [Online]. Available: https://ww2.arb.ca.gov/sites/default/files/barcu/board/books/2022/082522/prores22-12.pdf

[27] "Global car sales estimates". [Online]. Available: https://canalys.com/newsroom/canalys-global-electric-vehicle-sales-2020

[28] L. Spangher, W. Gorman, G. Bauer, Y. Xu, and C. Atkinson, "Quantifying the impact of us electric vehicle sales on light-duty vehicle fleet co2 emissions using a novel agent-based simulation," *Transportation Research Part D: Transport and Environment*, vol. 72, pp. 358–377, 2019.

[29] "EEI Projects 26 Million Electric Vehicles Will be on US Roads in 2030". [Online]. Available: https://www.eei.org/News/news/All/eei-projects-26-million-electric-vehicles-will-be-on-us-roads-in-2030#:~:text=The%20number%20of%20EVs%20on,on%20U.S.%20roads%20in%202030.

[30] "Are You Ready for the Future with Electric Trucks and Electric Buses?". [Online]. Available: https://www.electrotempo.com/wp-content/uploads/2022/09/Samuel-McKirahan-Technical-Paper-TSDOS.pdf

[31] [Online]. Available: https://electricgrids.engr.tamu.edu/electric-grid-test-cases/datasets-for-arpa-e-perform-program/

[32] "Electric Reliability Council of Texas Long-Term System Assessment". [Online]. Available: http://www.ercot.com/content/wcm/key_documents_lists/189719/2020_LTSA_Update_May2020_v3.pdf

[33] Houston-Galveston Area Council, "Regional travel models: 2016 model validation and documentation report," Houston-Galveston Area Council, Tech. Rep., March 2019.

[34] J. L. Wert, K. S. Shetye, H. Li, J. H. Yeo, X. Xu, A. Meitiv, Y. Xu, and T. J. Overbye, "Coupled infrastructure simulation of electric grid and transportation networks," in *2021 IEEE Power & Energy Society Innovative Smart Grid Technologies Conference (ISGT)*, 2021.

[35] K. S. Shetye, H. Li, J. L. Wert, X. Xu, A. Meitiv, Y. Xu, and T. J. Overbye, "Generation Dispatch and Power Grid Emission Impacts of Transportation Electrification," in *2021 North American Power Symposium (NAPS)*, 2021, pp. 01–06.

[36] Q.-S. Jia and T. Long, "A review on charging behavior of electric vehicles: data, model, and control," *Control Theory and Technology*, vol. 18, no. 3, pp. 217–230, Aug 2020. [Online]. Available: https://doi.org/10.1007/s11768-020-0048-8

[37] A. Meitiv, "Commercial vehicle trip generator based on the houston-galveston area council survey," *CARTEEH DATA:HUB*, 2021. [Online]. Available: http://carteehdata.org/library/dataset/commercial-vehicle-trip-g-94c7(accessedFeb012022)

[38] (2020) "Why most eTrucks will choose overnight charging". [Online]. Available: https://www.mckinsey.com/industries/automotive-and-assembly/our-insights/why-most-etrucks-will-choose-overnight-charging

[39] H. Li, A. L. Bornsheuer, T. Xu, A. B. Birchfield, and T. J. Overbye, "Load modeling in synthetic electric grids," in *2018 IEEE Texas Power and Energy Conference (TPEC)*. IEEE, 2018, pp. 1–6.

[40] H. Li, J. H. Yeo, A. L. Bornsheuer, and T. J. Overbye, "The creation and validation of load time series for synthetic electric power systems," *IEEE Transactions on Power Systems*, vol. 36, no. 2, pp. 961–969, 2020.

[41] A. Wood, B. Wollenberg, and G. Sheblé, *Power Generation, Operation, and Control*. Wiley, 2013. [Online]. Available: https://books.google.com/books?id=JDVmAgAAQBAJ

[42] M. F. Anjos, A. J. Conejo *et al.*, "Unit commitment in electric energy systems," *Foundations and Trends® in Electric Energy Systems*, vol. 1, no. 4, pp. 220–310, 2017.

[43] K. Hara, M. Kimura, and N. Honda, "A method for planning economic unit commitment and maintenance of thermal power systems," *IEEE Transactions on Power Apparatus and Systems*, no. 5, pp. 427–436, 1966.

[44] R. Kerr, J. Scheidt, A. Fontanna, and J. Wiley, "Unit commitment," *IEEE Transactions on Power Apparatus and Systems*, no. 5, pp. 417–421, 1966.

[45] F. Safdarian, A. Mohammadi, and A. Kargarian, "Temporal decomposition for security-constrained unit commitment," *IEEE Transactions on Power Systems*, vol. 35, no. 3, pp. 1834–1845, 2019.

[46] D. Bienstock and A. Verma, "Strong np-hardness of ac power flows feasibility," *Operations Research Letters*, vol. 47, no. 6, pp. 494–501, 2019.

[47] K. Lehmann, A. Grastien, and P. Van Hentenryck, "Ac-feasibility on tree networks is np-hard," *IEEE Transactions on Power Systems*, vol. 31, no. 1, pp. 798–801, 2015.

[48] T. J. Overbye, F. Safdarian, W. Trinh, J. H. Yeo, Z. Mao, and J. Snodgrass, "An approach for the direct inclusion of weather information in the power flow," in *Hawaii International Conference on System Sciences (HICSS)*, 2023.

[49] J. L. Wert, T. Chen, F. Safdarian, J. Snodgrass, and T. J. Overbye, "Calculation and validation of weather-informed renewable generator capacities in the identification of renewable resource droughts," in *15th IEEE PowerTech 2023*, 2023.

[50] M. Jereminov, A. Pandey, and L. Pileggi, "Equivalent circuit formulation for solving ac optimal power flow," *IEEE Transactions on Power Systems*, vol. 34, no. 3, pp. 2354–2365, 2019.
[51] Center for Disease Control (CDC), "Air pollutants." [Online]. Available: http://https://www.cdc.gov/air/pollutants.htm.
[52] M. Wang, A. Elgowainy, P. T. Benavides, A. Burnham, H. Cai, Q. Dai, T. R. Hawkins, J. C. Kelly, H. Kwon, D.-Y. Lee, U. Lee, Z. Lu, and L. Ou, "Summary of expansions and updates in GREET® 2018." [Online]. Available: https://www.osti.gov/biblio/1483843
[53] H. Cai, M. Wang, A. Elgowainy, and J. Han, "Updated greenhouse gas and criteria air pollutant emission factors and their probability distribution functions for electricity generating units." [Online]. Available: https://www.osti.gov/biblio/1045758
[54] "Transportation Conformity," 2019. [Online]. Available: https://www.h-gac.com/transportation-conformity/2019
[55] A. L. Meitiv and Y. A. Xu, "Tailpipe emission benefits of medium- and heavy-duty truck electrification in houston," 2020.
[56] GHG Emission Factors Hub. [Online]. Available: https://www.epa.gov/climateleadership/ghg-emission-factors-hub
[57] "Estimated U.S. Average Vehicle Emissions Rates per Vehicle by Vehicle Type Using Gasoline and Diesel". [Online]. Available: https://www.bts.gov/content/estimated-national-average-vehicle-emissions-rates-vehicle-vehicle-type-using-gasoline-and
[58] Greenhouse Gas Emissions from a Typical Passenger Vehicle. [Online]. Available: https://www.epa.gov/greenvehicles/greenhouse-gas-emissions-typical-passenger-vehicle
[59] L. Wilson. Calculate Your Driving Emissions. [Online]. Available: https://shrinkthatfootprint.com/calculate-your-driving-emissions/
[60] "Form EIA-860," 2020. [Online]. Available: https://www.eia.gov/electricity/data/eia860/
[61] A. B. Birchfield, K. M. Gegner, T. Xu, K. S. Shetye, and T. J. Overbye, "Statistical considerations in the creation of realistic synthetic power grids for geomagnetic disturbance studies," *IEEE Transactions on Power Systems*, vol. 32, no. 2, pp. 1502–1510, 2017.
[62] K. M. Gegner, A. B. Birchfield, T. Xu, K. S. Shetye, and T. J. Overbye, "A methodology for the creation of geographically realistic synthetic power flow models," in *2016 IEEE Power and Energy Conference at Illinois (PECI)*. IEEE, 2016, pp. 1–6.
[63] T. Xu, A. B. Birchfield, K. M. Gegner, K. S. Shetye, and T. J. Overbye, "Application of large-scale synthetic power system models for energy economic studies," in *Proceedings of the 50th Hawaii International Conference on System Sciences*, 2017.
[64] A. B. Birchfield, E. Schweitzer, M. H. Athari, T. Xu, T. J. Overbye, A. Scaglione, and Z. Wang, "A metric-based validation process to assess the realism of synthetic power grids," *Energies*, vol. 10, no. 8, 2017. [Online]. Available: https://www.mdpi.com/1996-1073/10/8/1233
[65] [Online]. Available: https://www.evolvehouston.org/rise-houston
[66] (2021) Justice40 Initiative. [Online]. Available: https://www.energy.gov/diversity/justice40-initiative

Jessica L. Wert (S'18) received the B.S. degree in engineering sciences from Smith College, Northampton, MA, USA, in 2018. She is currently working toward the Ph.D. degree in electrical engineering at Texas A&M University, College Station, TX, USA.

Farnaz Safdarian is a senior researcher at Texas A&M University, College Station, TX, USA. She received her Ph.D. in Electrical Engineering at Louisiana State University and her B.S. and M.S. degrees in Electrical Engineering, from Amirkabir University of Technology (Tehran Polytechnic) and Shahid Beheshti University, Iran, in 2011 and 2014, respectively.

Diana Wallison received the B.S. degree in electrical engineering from Texas A&M University, TX, USA, in 2017. She is currently pursuing a Ph.D. degree in electrical and computer engineering with Texas A&M University, TX, USA. Her research interests include co-simulation modeling and simulation, interactive simulation, dynamic load modeling and time-series simulation.

Jung Kyo Jung is a Master's student at Texas A&M University, College Station, TX, USA, 2021–2023. He has worked as a Senior Manager for KEPCO (Korea Electric Power Corporation), Seoul, Korea, 2006–2021. He received his B.E. in Electrical Engineering from Hongik University, Korea, in 2006.

Yijing Liu (S'17–M'22) received her B.S. degree from University of Electronic Science and Technology of China, Chengdu, P.R.C., and Ph.D. degree in Electrical and Computer Engineering from Texas A&M University, College Station, Texas, USA. Her research interests include power system dynamics modeling, renewable resources modeling and grid integration, and energy market.

Thomas J. Overbye (S'87-M'92-SM'96-F'05) received B.S., M.S., and Ph.D. degrees in electrical engineering from the University of Wisconsin Madison, Madison, WI, USA. He is currently with Texas A&M University where he is a Professor and holder of the O'Donnell Foundation Chair III.

Yanzhi (Ann) Xu is Cofounder and CEO of ElectroTempo, Inc. in Arlington, VA, USA. She received her Ph.D. in Transportation Systems Engineering from Georgia Institute of Technology in Atlanta, GA, USA in 2010 and her B.S. degree in Environmental Science from Peking University in Beijing, China in 2006.